UCRL-JRNL-216408

Compton Scattering X-Ray Sources Driven by Laser Wakefield Acceleration

F. V. Hartemann, D. J. Gibson, W. J. Brown, A. Rousse, K. T. Phuoc, and A. Pukhov

October 20, 2005

Physical Review Special Topics: Accelerators and Beams

Disclaimer

Compton Scattering X-Ray Sources Driven by Laser Wakefield Acceleration

F.V. Hartemann, D.J. Gibson, W.J. Brown*

Lawrence Livermore National Laboratory, Livermore, CA 94550

A. Rousse, K. Ta Phuoc

Ecole Nationale Supérieure des Techniques Avancées,

Laboratoire d'Optique Appliquée, 91761 Palaiseau, France

A. Pukhov

Institute for Theoretische Physik I, University of Dusseldorf, 40225 Dusseldorf, Germany

Abstract

Recent laser wakefield acceleration experiments have demonstrated the generation of femtosecond, nano-Coulomb, low emittance, nearly monokinetic relativistic electron bunches of sufficient quality to produce bright, tunable, ultrafast x-rays via Compton scattering. Design parameters for a proof-of-concept experiment are presented using a three-dimensional Compton scattering code and a laser-plasma interaction particle-in-cell code modeling the wakefield acceleration process; x-ray fluxes exceeding 10^{22} s^{-1} are predicted, with a peak brightness > 10^{20} photons / (mm^2 x $mrad^2$ x s x 0.1% bandwidth).

* Current address: Lincoln Laboratory, MIT, Lexington, MA 02420

PACS: 41.75.Jv, 52.38.-r, 41.60. Cr, 41.60.-m, 41.50.+h

1. Introduction

The generation of bright, ultrafast, tunable, hard x-rays from truly tabletop systems is a research goal of considerable interest, currently pursued by a number of groups worldwide. Such novel x-ray sources would have a wide variety of applications, ranging from dynamic diffraction studies of laser-pumped materials on the femtosecond time-scale, to time-resolved molecular dynamics [1-4] and advanced biomedical imaging [5].

Amongst different proposed schemes to generate ultrafast x-rays, such as laser-driven K_α sources [2,6-8], high-harmonic generation [9], or free-electron lasers [10], Compton scattering possesses a unique set of valuable characteristics, including compactness, wide tunability, femtosecond time-scale, and the potential for high brightness. This method has already been demonstrated using picosecond and femtosecond lasers synchronized to an rf linear accelerator (linac) [11-15]. Intense picosecond x-ray beams can be obtained in that case using head-on interaction geometries. The duration of the x-ray pulses depends on size of the interaction area, which fully depends on the size of the laser and particle beams as well as the angle of interaction. Different crossing techniques can then be used to keep the electron-photon superposition area small enough and produce subpicosecond x-ray pulses [16]; however, the x-ray flux becomes strongly diminished if the entire electron beam does not overlap with the laser pulse to produce the Compton scattering radiation.

Recently, three different groups [17-19] have demonstrated the successful production of high charge (nC), high energy (> 50 MeV), nearly monokinetic ($\Delta\gamma/\gamma \leq 10\%$) laser-produced plasma electron bunches using terawatt-class, few Joules, 30 fs chirped-pulse amplification (CPA) laser systems. These electron beams have a low divergence angle (few mrad), and the source size is very small (few μm); thus, the normalized emittance is comparable to, or better than, that obtained in conventional high-brightness linacs. Furthermore, the electron pulse duration is extremely short, of the order of a few tens of femtoseconds; this unique set of characteristics opens the path toward practical, compact, high brightness hard x-ray sources such as the all-optical Compton scattering scheme discussed in this paper.

The design parameters of a proof-of-principle experiment are presented, whereby hard x-rays are generated by colliding ultrashort electron bunches obtained via laser wakefield acceleration (LWFA) with laser pulses produced by a TW-class chirped-pulse amplification (CPA) laser, as shown schematically in Fig. 1. The advantages of using laser acceleration to produce the relativistic electrons are manifold: first, the ~ 1 nC electron bunches produced in this manner are extremely short, thus leading to intense femtosecond x-ray flashes by using of the entire electron bunch charge; second, the electrons can be synchronized with the Compton scattering drive laser with great accuracy; third, LWFA is a high-gradient process, allowing for a very compact system; finally, sufficiently low emittance and monokinetic beams can produce bright, broadband x-ray pulses that could be used for a number of interesting applications, including femtosecond Laue diffraction.

In Compton scattering, the basic interaction relies on the double Doppler upshift of incident photons by relativistic electrons: for head-on collisions, the energy of the scattered x-rays is given by $\hbar\omega_x$ ` $4\gamma^2\hbar\omega_0$, where $\gamma = 1 + eV / m_0c^2$ is the relativistic factor of the electrons accelerated to a potential *V*, and ω_0 is the frequency of the incident light. For example, for 800 nm light produced by a Ti:Al_2O_3 laser, the incident photon energy is 1.55 eV; a 50 MeV electron beam will generate 60 keV x-rays for head-on collisions. In addition, for the same interaction geometry, the x-ray pulse duration is essentially equal to the electron bunch length, thus offering the potential to generate femtosecond x-ray flashes; this particular interaction geometry offers other advantages over crossed beams setups, including better overlap and higher x-ray dose, as well as improved performance against timing jitter. Because the interaction is based on the relativistic Doppler effect, however, the electron beam quality plays an important role in the brightness of the x-rays.

In this paper, the properties of the electron beam used for the Compton scattering calculations are derived from three-dimensional (3D) particle-in-cell (PIC) simulations that fit the experimental data of the more recent LWFA experiments [17]. The brightness scaling of Compton scattering and other salient theoretical features are then briefly outlined, and the 3D time and frequency domain Compton scattering code structure is discussed; this code has been extensively benchmarked against recent Compton scattering experiments performed at Lawrence Livermore National Laboratory (LLNL) using a 150 MeV linac and a high-brightness S-band photoinjector. Finally, the two codes are interfaced to predict the properties of the x-ray pulses that a Compton scattering source driven by laser wakefield acceleration will produce experimentally, and conclusions are drawn.

2. Electron beam parameters

Three-dimensional (3D) particle-in-cell (PIC) simulations using the code “Virtual Laser Plasma Laboratory” [20,21] were used to closely match the data of the recent LWFA experiments [17]; these LWFA parameters are shown in Table 1. The few percent energy spread of the electron beam results from the highly nonlinear interaction of the laser with the plasma. As the pulse propagates in the plateau region of a gas jet, it self-focuses and undergoes longitudinal compression by plasma waves. This decreases the effective radius of the laser pulse and increases the laser intensity by one order of magnitude. This compressed laser pulse is now resonant with the plasma wave and it drives a highly nonlinear wakefield: the laser ponderomotive potential expels the plasma electrons radially and leaves a cavitated region behind (this is referred to as the 'cavitation' or 'blow-out' regime). In this regime, the 3D structure of the wakefield resembles a plasma bubble. As the electron density at the walls of the bubble becomes large, wave-breaking occurs and electrons are injected and accelerated inside the bubble. As the number of trapped electrons increases, the bubble elongates. Its effective group velocity decreases, and electrons start to dephase with respect to the accelerating field. This dephasing causes electron self-bunching in phase space, which results in the monoenergetic peak in the energy spectrum.

Table 1 LWFA parameters from Ref. [17].

Drive laser pulse wavelength	800 nm
Drive laser pulse energy	1 J
Drive laser pulse duration	21 fs
Plasma density	1.0×10^{18} cm^{-3}
Electron bunch charge	0.5 nC
Electron bunch duration	12 fs

Electron bunch energy	170 MeV
Relative energy spread	5 %
Electron bunch divergence	10 mrad

3. Brightness scaling, basic Compton scattering physics

In Compton scattering, the Doppler upshifted frequency of the scattered radiation can be readily determined by considering energy-momentum conservation: $m_0 c u_\mu^0 + \hbar k_\mu^0 = m_0 c u_\mu^s + \hbar k_\mu^s$, where u_μ^0 is the electron 4-velocity before the interaction, k_μ^0 is the 4-wavenumber of the incident photon, and where u_μ^s and k_μ^s are the corresponding quantities after the scattering event. Using the normalization of the 4-velocity, $u_\mu u^\mu = \mathbf{u}^2 - \gamma^2 = -1$, and the photon mass shell condition, or vacuum dispersion relation, $k_\mu k^\mu = 0$, one finds that: $k_\mu^s \left(u_\mu^0 + \bar{\lambda}_C k_\mu^0 \right) = k_\mu^0 u_0^\mu$. In vector form, this result can be expressed as:

$$k_s = \frac{\gamma_0 k_0 - \mathbf{u}_0 \cdot \mathbf{k}_0}{\left(\gamma_{0k_0} + \bar{\lambda}_C k_0 \right) - \hat{\mathbf{n}}_s \cdot \left(\mathbf{u}_0 + \bar{\lambda}_C \mathbf{k}_0 \right)}, \tag{1}$$

where $\hat{\mathbf{n}}_s$ is the direction of observation. In the case where recoil is negligible, we have $\bar{\lambda}_C k_0 \ll 1$, and one recovers the well-known Doppler effect:

$$\frac{k_s}{k_0} = \frac{\gamma_0 - u_0 \cos\varphi}{\gamma_0 - u_0 \cos\theta}, \tag{2}$$

where φ and θ are the incidence and scattering angles, respectively. For head-on collisions, $\varphi = \pi$, and the maximum Doppler upshift is obtained along the electron velocity, at $\theta = 0$: $k_s = k_0\left(\gamma_0 + u_0\right)/\left(\gamma_0 - u_0\right)$ ` $4\gamma_0^2 k_0$.

The local number of x-ray photons scattered per unit time and volume is given by the product of the electron beam 4-current, $j_\mu\left(x_\nu\right) = ecn_e\left(x_\nu\right)u_\mu/\gamma$, and the incident photon 4-flux, $\Phi_\mu\left(x_\nu\right) = cn_\lambda\left(x_\nu\right)k_\mu/\omega$:

$$\frac{d^4N_x\left(x_\nu\right)}{d^4x_\nu} = \frac{\sigma}{ec} j_\mu\left(x_\nu\right)\Phi^\mu\left(x_\nu\right) = \frac{\sigma c}{\gamma\omega} n_e\left(x_\nu\right)n_\lambda\left(x_\nu\right)u_\mu k^\mu. \tag{3}$$

Here, $u_\mu = dx_\mu/cd\tau = \left(\gamma, \mathbf{u}\right)$ is the electron 4-velocity, $k_\mu = \left(\omega/c, \mathbf{k}\right)$ is the incident photon 4-wavenumber, and $\sigma = 8\pi r_0^2/3$ is the Compton scattering cross-section, expressed in terms of the classical electron radius, $r_0 = e^2/4\pi\varepsilon_0 m_0 c^2 = 2.8178\times10^{-15}$ m.

Near the focal region, the electron beam density can be described by

$$n_e(r,z,t) = \frac{N_e}{\sqrt{\pi}^3 c\Delta\tau r_b^2} \frac{1}{1+\left(k_f z\right)^2} \exp\left\{-\left(\frac{t - \frac{u_0 z}{\gamma_0 c}}{\Delta\tau}\right)^2 - \frac{r^2}{r_b^2\left[1+\left(k_f z\right)^2\right]}\right\}, \tag{4}$$

where $N_e = q/e$ is the number of electrons in the bunch, $\Delta\tau$ is the bunch duration, r_b is the radius at focus, and where the inverse beta-function is given in terms of the normalized emittance, ε, beam focal radius, and energy, γ_0, by $k_f = \beta_f^{-1} = \varepsilon / \gamma_0 r_b^2$. Similarly, the photon density of the focusing and diffracting laser pulse is described by

$$n_\lambda(r,z,t) = \frac{N_\lambda}{\sqrt{\frac{\pi}{2}}^{3} c\Delta t w_0^2} \frac{1}{1+\left(\frac{z}{z_0}\right)^2} \exp\left\{-2\left(\frac{t+\frac{z}{c}}{\Delta t}\right)^2 - 2\frac{r^2}{w_0^2\left[1+\left(\frac{z}{z_0}\right)^2\right]}\right\}, \tag{5}$$

where $N_\lambda = W/\hbar\omega_0$ is the total number of photons in the laser pulse, Δt is the pulse duration, and is related to the bandwidth as $\Delta t \Delta\omega = \sqrt{2}$, in the case of a Fourier transform-limited pulse, w_0 is the $1/e^2$ focal radius, and $z_0 = \pi w_0^2/\lambda_0$ is the associated Rayleigh length.

The on-axis flux can then be derived analytically from Eq. (3):

$$\frac{dN_x}{dt_d} \grave{} \; \frac{8}{3}\frac{r_0^2}{w_0^2}(1+\beta_0)\frac{N_e N_\lambda}{\Delta\tau}\mathscr{F}(\xi,\eta,\mu)\exp\left[-\left(\frac{t_d}{\Delta\tau}\right)^2\right] = \frac{N_x}{\sqrt{\pi}\Delta\tau}e^{-t_d^2/\Delta\tau^2}, \tag{6}$$

where we have defined the normalized inverse beta-function, $\eta = k_f c\Delta t/2\sqrt{2}$, the normalized inverse Rayleigh length, $\mu = c\Delta t/2\sqrt{2}z_0$, $\xi\mu/\eta = 2r_b^2/w_0^2$, the overlap function,

$$\mathcal{F}(\xi,\eta,\mu)=\frac{\left[1-\Phi\left(\sqrt{\frac{\eta+\xi\mu}{\eta\mu^2+\xi\mu\eta^2}}\right)\right]}{\sqrt{\left(\mu^2+\xi\mu\eta\right)\left(1+\xi\frac{\mu}{\eta}\right)}}\exp\left(\frac{\eta+\xi\mu}{\eta\mu^2+\xi\mu\eta^2}\right), \tag{7}$$

and the integrated dose,

$$N_x \approx \frac{8\sqrt{\pi}}{3}\frac{r_0^2}{w_0^2}\left(1+\beta_0\right)N_e N_\lambda \mathcal{F}(\xi,\eta,\mu). \tag{8}$$

Equation (6) shows that the x-ray pulse duration is essentially equal to that of the electron bunch for head-on collisions.

The details of the derivations leading to the results given above can be found in Ref. [22].

Starting from Eq. (3), the peak brightness can also be derived under the assumption that the energy spread and emittance remain small:

$$\begin{aligned}\hat{B}_x &= \frac{4\times10^{-15}}{\pi^2}\frac{\gamma_0^2}{\varepsilon^2}\frac{N_e N_\lambda}{\Delta\tau}\frac{r_0^2}{w_0^2}\exp\left\{\frac{\chi-1}{2\chi\Delta u_\perp^2}\left[2+\frac{\delta\omega^2+\delta\gamma^2\chi^2}{2\chi(\chi-1)\Delta u_\perp^2}\right]\right\}\\ &\times\left\{1-\Phi\left\{\frac{\chi-1}{\sqrt{\delta\omega^2+\delta\gamma^2\chi^2}}\left[1+\frac{\delta\omega^2+\delta\gamma^2\chi^2}{2\chi(\chi-1)\Delta u_\perp^2}\right]\right\}\right\}\left\{\frac{\eta e^{\frac{1}{\eta^2}}\left[\Phi\left(\frac{1}{\eta}\right)-1\right]-\mu e^{\frac{1}{\mu^2}}\left[\Phi\left(\frac{1}{\mu}\right)-1\right]}{\mu^2-\eta^2}\right\}.\end{aligned} \tag{9}$$

Here, $\chi = \omega_x / 4\gamma_0^2\omega_0$ is the normalized Doppler-upshifted frequency, $\delta\omega = \Delta\omega/\omega_0$ is the relative spectral width of the drive laser pulse, and $\delta\gamma = 2\Delta\gamma/\gamma_0$ is the scaled relative energy spread; $\Delta u_\perp r_b = \varepsilon u_0 / \gamma_0$ ` ε.

This result clearly underscores the importance of the electron beam quality: the x-ray brightness is proportional to that of the electron bunch. In particular, the x-ray brightness scales inversely quadratically with the physical emittance, ε / γ_0, and linearly with the electron bunch focused current density. Therefore, the ultrashort, high charge, low emittance electron beams produced by laser wakefield acceleration are good candidates to drive compact Compton scattering x-ray sources, provided their energy spread is sufficiently low.

4. Three-dimensional time and frequency domain x-ray code

A very detailed description of the three-dimensional time and frequency domain x-ray code used here to model the main characteristics of the radiation produced by colliding a relativistic electron bunch produced by LWFA with an intense laser pulse is given in Ref. [23]; in the present paper, a brief overview is given for completeness.

Starting from the local number of x-ray photons scattered per unit time and volume, as expressed in Eq. (3), one can obtain the radiated x-ray density per unit solid angle by using the differential scattering cross-section:

$$\frac{d^5 N_x}{d^4 x_\mu d\Omega_x} = \frac{d\sigma}{d\Omega_x} c \frac{u_\nu k^\nu}{\gamma\omega} n_\lambda\left(x_\mu\right) n_e\left(x_\mu\right). \tag{10}$$

The local spectral brightness can be derived by using the Doppler-shifted x-ray frequency, which is given by Eq. (2) in the Thomson limit; we then have

$$\frac{d^6 N_x}{d^4 x_\mu d\Omega_x d\omega_x} = \frac{d\sigma}{d\Omega_x}\left(1 - \boldsymbol{\beta}\cdot\frac{c\mathbf{k}}{\omega}\right) n_\lambda\left(x_\mu\right) n_e\left(x_\mu\right) \delta\left(\omega_x - \omega\frac{\kappa}{\kappa_x}\right), \tag{11}$$

where $\kappa = \gamma - \mathbf{u}\cdot\frac{c\mathbf{k}}{\omega}$ and $\kappa_x = \gamma - \mathbf{u}\cdot\hat{\mathbf{n}}_x$ are the electron light-cone variables with respect to the incident and scattered photons, respectively.

For realistic electron and laser beams, Eq. (11) must be integrated over the entire phase space of each beam to yield the corresponding x-ray brightness, within the context of an incoherent superposition. A general expression for the differential cross section in Eq. (11) can be derived by first transforming the wave vector of incident photon into the electron rest frame; the corresponding rest frame differential cross section can then be transformed back into the lab frame.

In its most general form, the program calculates the number of photons scattered into a given solid angle and within a range of scattered frequencies at each time step by summing over all incident wave-vectors within the laser pulse, which accurately models the laser pulse phase space. This is performed for all the electrons in the bunch, which are represented by a series of macro-particles with a charge-to-mass ratio equal to e/m_0. Furthermore, the zeroth-order (no laser) electron motion through the laser focus is assumed to be ballistic, which is a good assumption given the fact that the relativistic plasma wavelength of the electron bunch is much longer than all other scale lengths. Within this context, the input to the code is a table listing the 6-dimensional position and momentum coordinates of each macro-particle at a given time; from that data, the macro-particles are ballistically propagated until they are subjected to the incident laser pulse, and scattering occurs. The temporal information of the x-ray pulse is calculated from the time of the interaction at each time step in conjunction with the time of flight of the produced photon to the detector at a specified distance to the interaction. Spatial information of the scattered x-ray pulses can be determined by performing this calculation for several different observation angles.

The three-dimensional code described above has been thoroughly benchmarked against ongoing Compton scattering experiments at LLNL [11,24-25]. For example, Fig. 2 shows the excellent agreement obtained between the three-dimensional codes and the experimentally measured angular x-ray energy distribution. The integrated x-ray doses agree to within 10%. This deviation is attributed to the accuracy with which the various moments of the electron and laser phase spaces can be measured, including, energy, energy distribution, emittance, focal spot size, beta-function, Rayleigh range, and charge. For more detail, we refer the reader to reference [23].

5. X-ray simulations

As mentioned above, the input to the code is a table listing the 6-dimensional position and momentum coordinates of each macro-particle at a given time; for the simulations given here, that input is provided by the PIC code describing the LWFA process. Figures 3 and 4 show the LWFA electron phase space, as simulated by the PIC code. The phase space is highly correlated, probably because of the strong nonlinear electromagnetic fields present in the laser-driven plasma wakefield, as seen in Fig. 4.

The electron bunch produced by LWFA is also extremely short; thus, 180-degree Compton scattering will provide equally short x-ray flashes, of great potential interest to the users community; this is confirmed by the simulations, which show that a high photon dose can be produced: 1.65×10^{9} photons, in the particular case simulated here, with a peak flux exceeding 10^{23} photons/s. The x-ray spectrum shown in Fig. 5 is quite broad; this is due to the small spot size and relatively large divergence of the LWFA electron beam, which is also reflected in the x-ray beam, as shown in Fig. 6 (bottom); such broad spectra are ideal for ultrafast Laue diffraction experiments. The electron bunch temporal shape is faithfully reproduced in the x-ray pulse, as seen in Fig. 6 (top), which opens the possibility of preparing specific electron beam pulse shapes for different x-ray applications; in particular, double-pulsing the source on the femtosecond time-scale appears feasible, in principle. At this point, it is important to note that in the present simulations, no effort was made to capture and manipulate the LWFA beam prior to x-ray production; depending upon the quantity of interest to the users, different configurations could be proposed: for example, relatively narrow-band x-rays can be produced by increasing the electron beam size, while decreasing its divergence; on the other hand, for some other applications the x-ray source size could be minimized, at the expense of spectral purity. Under the electron beam conditions simulated here, the peak x-ray brightness exceeds 10^{20} photons / (mm^{2} x mrad^{2} x s x 0.1% bandwidth), which represents a very high value for such a compact system; the average brightness remains modest, but multi-Joule, 1kHz laser systems are currently under development, and could yield a path to improved average brightness, useful for advanced biomedical imaging and other advanced applications.

6. Conclusions

Following the recent demonstration of efficient, high quality electron beam acceleration in a laser wakefield, three-dimensional simulations have been performed to generate an accurate picture of the electron beam phase space, and to predict the x-ray output of LWFA-based Compton scattering experiments, where the electron beam collides with a fraction of the drive laser pulse to produce a very bright, femtosecond x-ray flash. Our study, using fully benchmarked codes, shows that high dose ($>10^9$ photons/shot), high peak brightness [> 10^{20} photons / (mm^2 x mrad^2 x s x 0.1% bandwidth)] x-ray pulses could be produced following that approach. As the LWFA electron beam is extremely short, the maximum photon flux predicted by the code exceeds 10^{23} photons/s, and opens a path to ultrafast Laue diffraction experiments, taking advantage of the broadband x-ray spectrum generated by Compton scattering. Finally, we note that the maximum x-ray energy produced in these simulations approaches 1 MeV, thus indicating that femtosecond positron pulses could also be generated by increasing either the LWFA electron beam energy or by frequency-multiplying the laser pulse used for Compton scattering to exceed the pair production threshold, and reach sufficiently large pair production cross-section in dense metallic targets.

Acknowledgements

This work was performed under the auspices of the U.S. Department of Energy by University of California, Lawrence Livermore National Laboratory under Contract W-

7405-Eng-48. One of us (FVH), would also like to acknowledge very useful discussions with D.T. Santa Maria.

References

1. N. Bloembergen, Rev. Mod. Phys. **71**, S283–S287 (1999).
2. A. Rousse *et al.*, Rev. Mod. Phys. **73** (1), 17-31 (2001).
3. http://tesla.desy.de/new_pages/TDR_CD/PartV/fel.html
4. http://www-ssrl.slac.stanford.edu/lcls/
5. J. Drenth, *Principles of Protein X-Ray Crystallography*, 2nd Ed. (Springer, New York, NY 1999).
6. A. Rousse *et al.*, Phys. Rev. **E50** (3), 2200 (1994).
7. Ch. Rischel *et al.*, Nature **390**, 490 (1997).
8. C.W. Siders, A. Cavalleri, K. Sokolowski-Tinten, Cs. Toth, T. Guo, M. Kammler, M. Horn von Hoegen, K. R. Wilson, D. von der Linde, and C.P.J. Barty, Science **286**, 1340 (1999).
9. R. Bartels, S. Backus, E. Zeek, L. Misoguti, G. Vdovin, I. P. Christov, M.M. Murnane, and H.C. Kapteyn, Nature **406**, 164 (2000).
10. J. Arthur, G. Materlik, R. Tatchyn, and H. Winick, Rev. Sci. Instrum. **66**, 1987 (1995).
11. D.J. Gibson, S.G. Anderson, C.P. J. Barty, S.M. Betts, R. Booth, W.J. Brown, J.K. Crane, R.R. Cross, D.N. Fittinghoff, F.V. Hartemann, J. Kuba, G.P. Le Sage, D.R. Slaughter, A.M. Tremaine, A.J. Wootton, E.P. Hartouni, P.T. Springer, and J.B. Rosenzweig, Phys. Plasmas **11**, 2857 (2004).
12. A. Ting *et al.*, Nucl. Instr. Methods Phys. Res. A 375 ABS68 (1996)

13. I.V. Pogorelsky *et al.*, Phys. Rev. ST Accel. Beams 3, 090 702 (2000)
14. W.P. Leemans *et al.*, Phys. Rev. Lett. **77**(20) 4182 (1996).
15. K. Chouffani *et al.*, Nucl. Instr. Methods Phys. Res. **A 495**, 95 (2002).
16. Y. Li *et al.*, Phys. Rev. STAB **5**, 0444701 (2002).
17. J. Faure, Y. Glinec, A. Pukhov, S. Kiselev, S. Gordienko, E. Lefebvre, J.-P. Rousseau, F. Burgy, and V. Malka, Nature **431**, 541 (2004).
18. S.P.D. Mangles, C.D. Murphy, Z. Najmudin, A.G.R. Thomas, J.L. Collier, A.E. Dangor, E.J. Divall, P.S. Foster, J.G. Gallacher, C.J. Hooker, D.A. Jaroszynski, A.J. Langley, W.B. Mori, P.A. Norreys, F.S. Tsung, R. Viskup, B.R. Walton, and K. Krushelnick, Nature **431**, 535 (2004).
19. C.G.R. Geddes, Cs. Toth, J. van Tilborg, E. Esarey, C. B. Schroeder, D. Bruhwiler, C. Nieter, J. Cary, and W.P. Leemans, Nature **431**, 538 (2004).
20. A. Pukhov and J. Meyer ter Vehn, Appl. Phys. B **74**, 355 (2002).
21. Kostyukov, A. Pukhov, and S. Kiselev, Phys. Plasmas **10**, 4818 (2003).
22. F.V. Hartemann, W.J. Brown, D.J. Gibson, S.G. Anderson, A.M. Tremaine, P.T. Springer, A.J. Wootton, E.P. Hartouni, and C.P.J. Barty, accepted for publication in Phys. Rev. STAB (2005).
23. W.J. Brown and F.V. Hartemann, Phys. Rev. STAB **7**, 060703 (2004).
24. W. J. Brown, S.G. Anderson, C. P. J. Barty, S. M. Betts, R. Booth, J.K. Crane, R.R. Cross, D.N. Fittinghoff, D.J. Gibson, F.V. Hartemann, E. P. Hartouni, J. Kuba, G. P. Le Sage, J. B. Rosenzweig, D. R. Slaughter, A.M. Tremaine, A.J. Wootton, and P.T. Springer, Phys. Rev. STAB **7**, 060702 (2004).

25. F.V. Hartemann, A.M. Tremaine, S.G. Anderson, C. P. J. Barty, S. M. Betts, R. Booth, W. J. Brown, J.K. Crane, R.R. Cross, D.J. Gibson, D.N. Fittinghoff, J. Kuba, G. P. Le Sage, D.R. Slaughter, A.J. Wootton, E. P. Hartouni, P.T. Springer, J.B. Rosenzweig, A.K. Kerman, Laser and Part. Beams **22**, 221 (2004).

Figure captions

Fig. 1 Schematic of a Compton scattering x-ray experiment using LWFA electrons. The energy of the x-rays, $\hbar\omega_x$, depends on the angle between the laser and electron beams, φ, as well as on the angle of observation from the electron beam direction, θ, and the electron energy, $\gamma m_0 c^2$.

Fig. 2 Comparison between the observed angular x-ray distribution (blue line), the 3D code (green line), for LLNL linac Compton scattering experiments (see Refs. [24] and [25]). The red line outlines the $1/\gamma$ energy-integrated cone.

Fig. 3 LWFA phase space, as simulated by 3D PIC code. Top: electron beam energy spectrum. Bottom: temporal electron pulse profile.

Fig. 4 LWFA transverse electron beam phase space, as simulated by 3D PIC code.

Fig. 5 On-axis x-ray spectrum, simulated by the three-dimensional time and frequency domain Compton scattering code, using the three-dimensional PIC code-generated electron beam phase space as an input.

Fig. 6 Top: temporal x-ray pulse shape, as simulated by the three-dimensional time and frequency domain Compton code, using the three-dimensional PIC code-generated electron beam phase space as an input. The temporal x-ray pulse (blue line) is superimposed on the temporal electron distribution to show the close correlation. Bottom: x-ray angular energy distribution.

Fig. 1

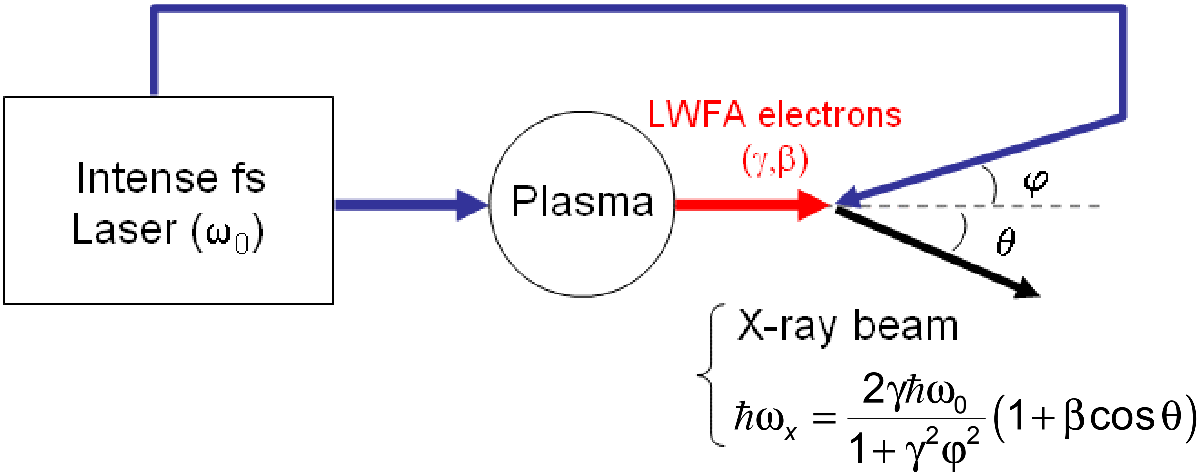
Intense fs Laser (ω_0)
Plasma
LWFA electrons
(γ,β)
φ
θ
X-ray beam
$\hbar\omega_x = \frac{2\gamma\hbar\omega_0}{1+\gamma^2\varphi^2}(1+\beta\cos\theta)$

Fig. 2

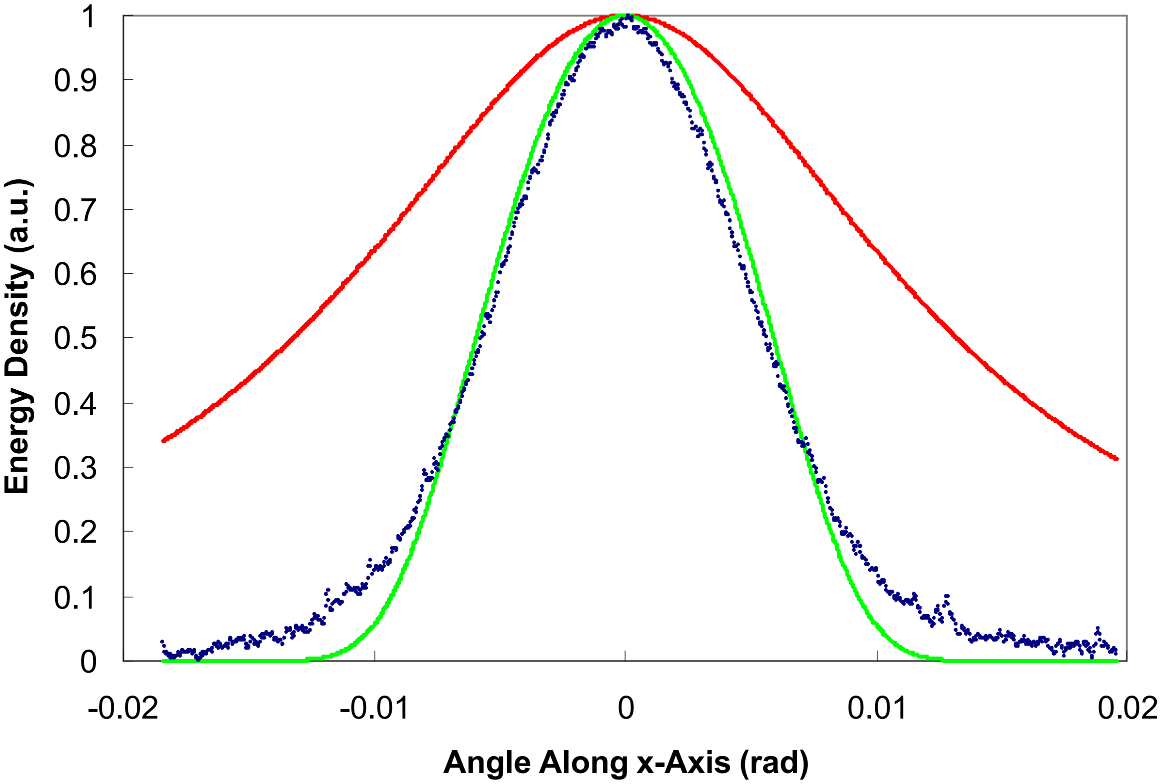
1
0.9
0.8
0.7
0.6
0.5
0.4
0.3
0.2
0.1
0
Energy Density (a.u.)
-0.02
-0.01
0
0.01
0.02
Angle Along x-Axis (rad)

Fig. 3

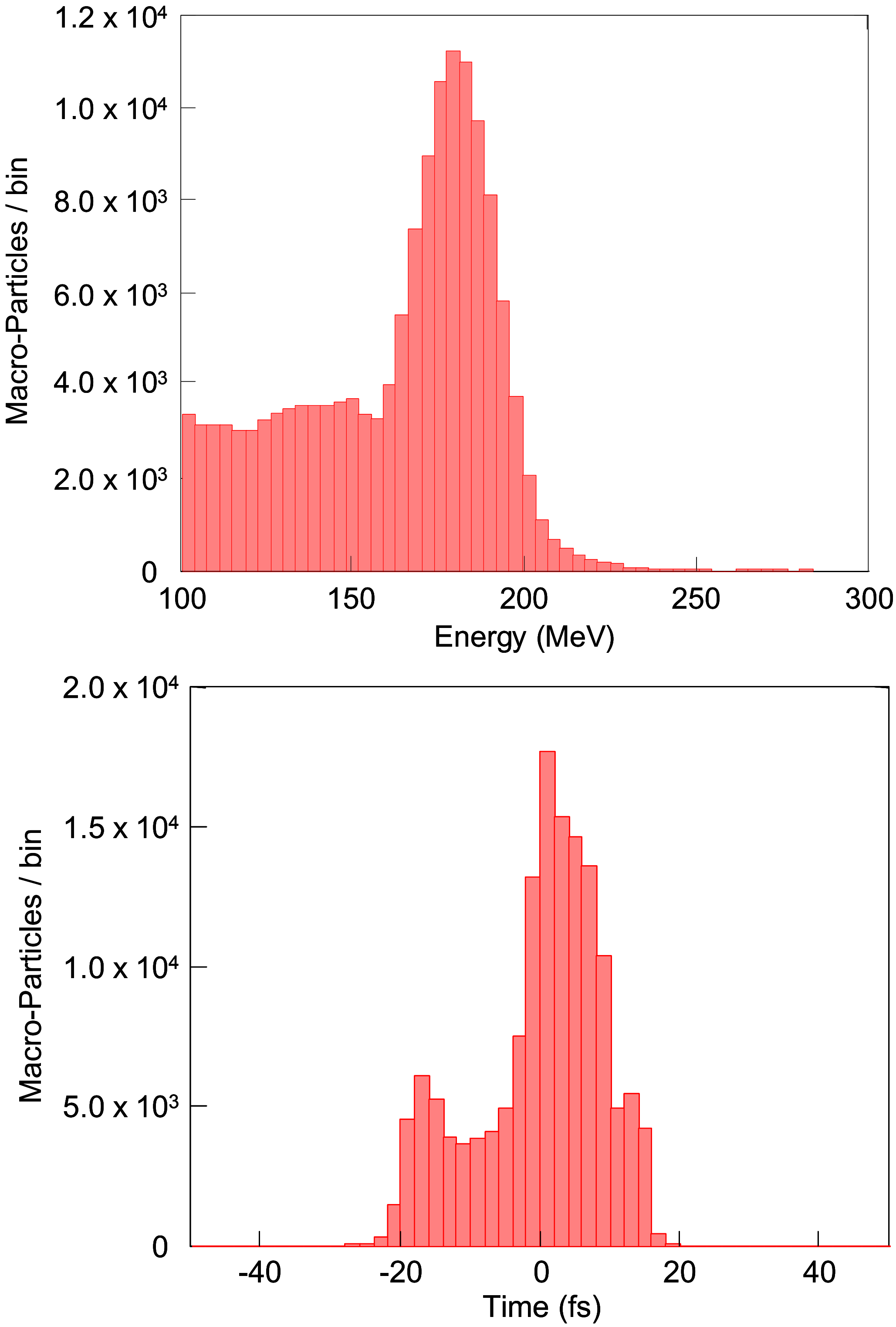

1.2 x 10⁴
1.0 x 10⁴
8.0 x 10³
6.0 x 10³
4.0 x 10³
2.0 x 10³
0
Macro-Particles / bin
100
150
200
250
300
Energy (MeV)
2.0 x 10⁴
1.5 x 10⁴
1.0 x 10⁴
5.0 x 10³
0
Macro-Particles / bin
-40
-20
0
20
40
Time (fs)

Fig. 4

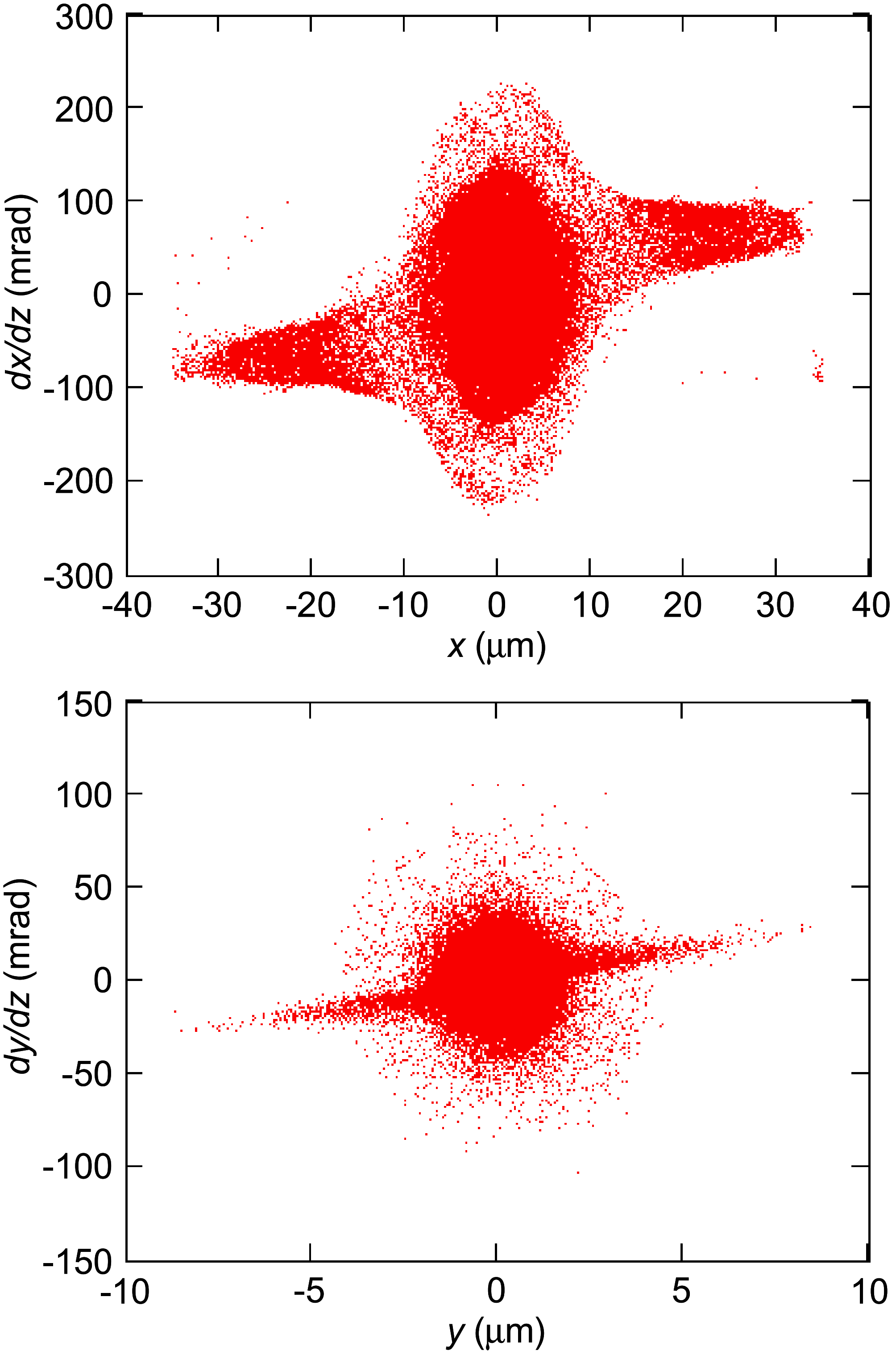

300
200
100
0
-100
-200
-300
dx/dz (mrad)
-40
-30
-20
-10
0
10
20
30
40
x (μm)
150
100
50
0
-50
-100
-150
dy/dz (mrad)
-10
-5
0
5
10
y (μm)

Fig. 5

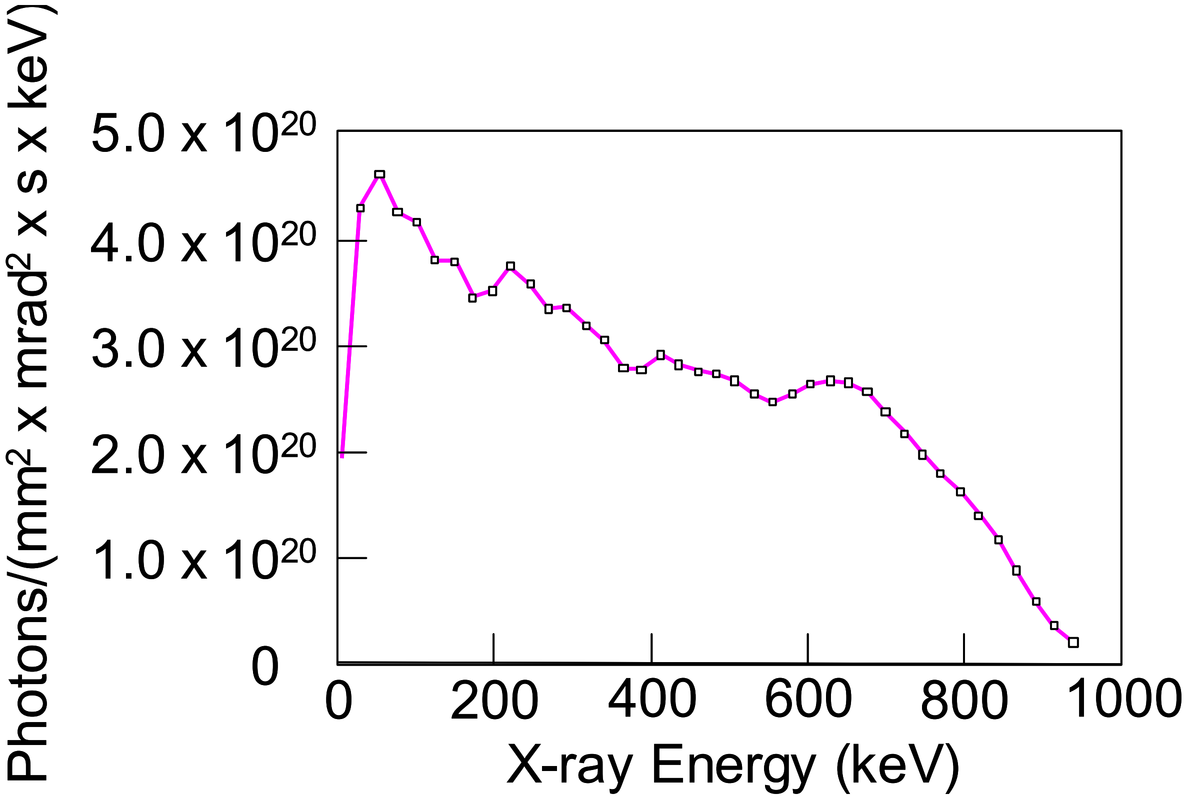

Photons/(mm^2 x mrad^2 x s x keV)
5.0 x 10^{20}
4.0 x 10^{20}
3.0 x 10^{20}
2.0 x 10^{20}
1.0 x 10^{20}
0
0
200
400
600
800
1000
X-ray Energy (keV)

Fig. 6

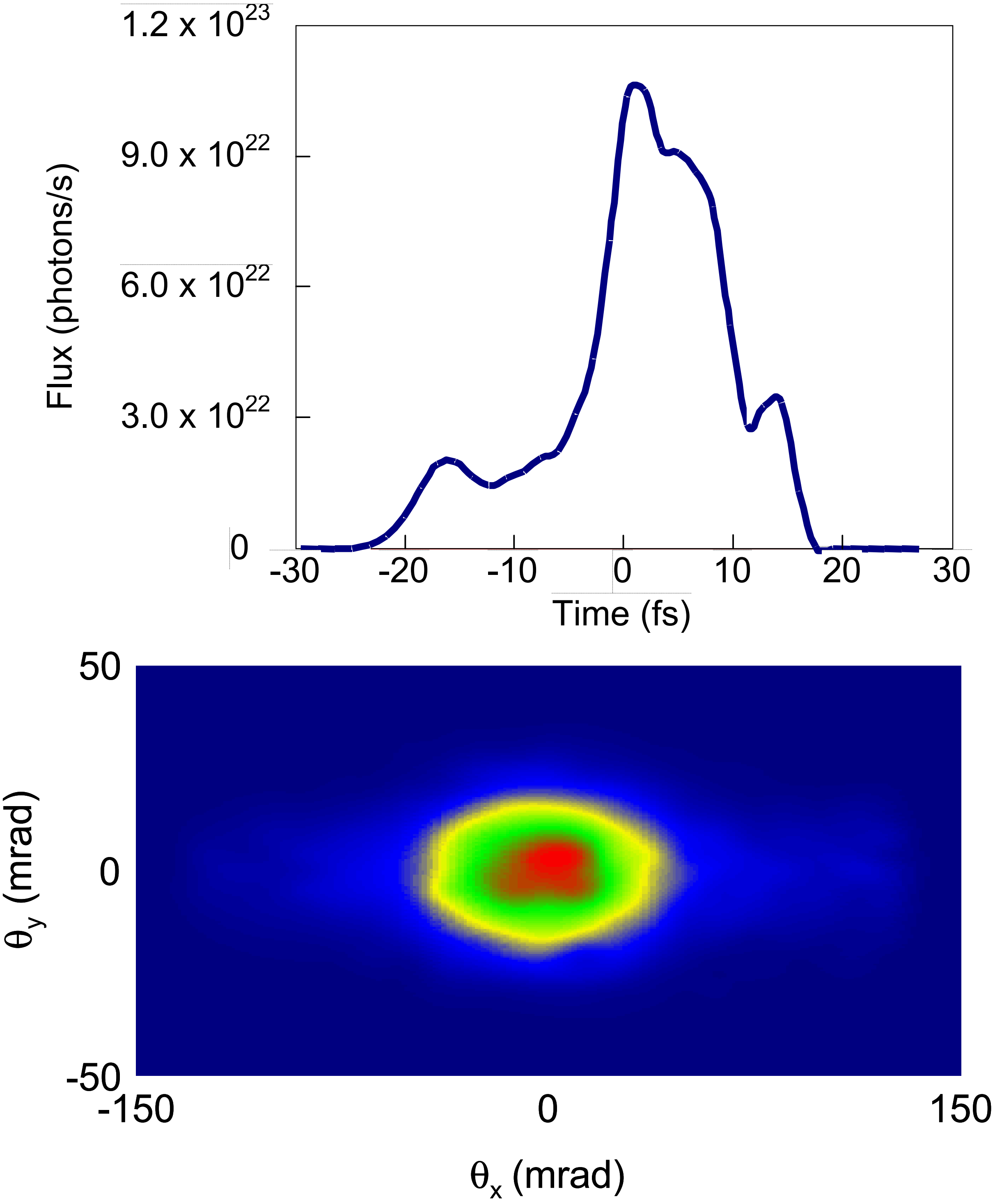
Flux (photons/s)
1.2 x 10^23
9.0 x 10^22
6.0 x 10^22
3.0 x 10^22
0
-30
-20
-10
0
10
20
30
Time (fs)
50
0
-50
θy (mrad)
-150
0
150
θx (mrad)